Transient Stability Analysis and Control of Grid-Forming Converters Under Current Limiting Based on Relative Kinetic Energy

Qin Gao[1], Yingjie Chen[3,*], Zhisheng Wang[2], Xinjian Zhang[1], Yong Mei[1], and Nan Zhang[1]
[1]System Operations Department, China Southern Power Dispatch and Control Center, Guangzhou City, Guangdong 510623, China
[2]Engineering Laboratory for Smart Operation and Control and Renewable Energy Grids, Ministry of Education (Northeast Electric Power University), Jilin 132012, China
[3]Smart Grid Protection and Operation Control Laboratory, NARI Group Corporation (State Grid Electric Power Research Institute Co., Ltd.), Nanjing 211106, China

Corresponding author: Yingjie Chen (e-mail: 15567583209@163.com).

ABSTRACT Under large disturbances, voltage-source inverters (VSIs) may experience transient power-angle instability similar to that of conventional synchronous machines; however, their limited overcurrent capability necessitates current-limiting mechanisms, under which the inverter may effectively behave as a current source, leading to more complex synchronization and stability challenges. To address transient instability induced by current saturation, this paper proposes an emergency control strategy based on the concept of relative kinetic energy, in which transient grid instability is identified in real time by analyzing the evolution of rotor speed deviation with respect to the virtual power angle. When impending angle instability is detected, the remaining acceleration area is calculated using relative kinetic energy theory, while the required active power adjustment is determined simultaneously, with the influence of control action delay explicitly incorporated to enhance reliability. Simulation results verify that the proposed strategy can effectively maintain system transient stability, and if the initial control action fails, a feedback-based closed-loop architecture can autonomously trigger secondary emergency control to ensure the system remains within a secure and stable operating region throughout the transient process. The proposed method eliminates the need for detailed modeling of power system components or explicit operating mode identification, relying only on measured generator power angles and rotor speeds to adapt to arbitrarily complex operating conditions and fault scenarios with low computational burden and high flexibility, thereby effectively preventing system deterioration and mitigating the risk of large-scale blackouts, which demonstrates strong practical engineering value for enhancing grid security and transient stability defense capabilities.

INDEX TERMS Grid-forming control, Transient stability, Emergency control, Relative kinetic energy.

I. INTRODUCTION

In the worldwide movement towards achieving carbon emissions' peak and carbon neutrality, a clear direction has been set for energy transition and sustainable economic development. The attainment of these objectives hinges on several critical priorities: The extensive adoption of renewable energy sources, improved energy efficiency measures, and ongoing enhancements and advancements in power system design [1-2]. The voltage source converter, as a pivotal power electronics technology, plays a crucial role in achieving the "dual carbon" goals [3-4]. Currently, most VSC-based renewable energy generation equipment adopts grid-following (GFL) control. Essentially operating in current-source control mode, GFL converters can precisely regulate active and reactive power outputs according to preset reference values. However, their control mechanism relies on the phase angle output from phase-locked loops (PLLs). Under transient low-voltage conditions, PLLs may fail to accurately track grid phase angles, resulting in transient instability risks for grid-following converters[5-7]. grid-forming (GFM) control has garnered significant attention as a viable solution for power system transformation. Operating inherently in voltage-source control mode, GFM converters autonomously regulate both voltage magnitude and phase angle through power synchronization mechanisms. This approach enables the delivery of required power output while maintaining grid-synchronized operation. Notably, GFM control demonstrates self-synchronization capability and stable performance in weak grid conditions[8-10]. Droop control has the same active power-frequency (P-f) and reactive power-voltage (Q-V) characteristics as synchronous generators and is one of the simplest and most widely used control strategies in grid-forming control strategies[11-12]. Droop control does not have the inertia and damping characteristics of synchronous generators. Therefore, droop control will cause grid voltage and frequency oscillation. In typical system disturbances, the frequency deviation and voltage fluctuation caused by droop control are relatively large, which brings great challenges to grid stability and security[13]. Virtual Synchronous Generator control emulates the electromechanical characteristics of synchronous generators, Compared to droop control, VSG control can simulate inertia, thereby enhancing the equivalent inertia level of the system[14-15]. Unlike traditional synchronous generators, the control parameters of Grid-Forming Voltage Source Converters are not constrained by physical limitations, and their overcurrent capability is far inferior to that of synchronous generators. Therefore, current-limiting strategies must be designed within the converter to prevent exceeding its overcurrent capacity during faults. However, under large disturbances, the inverter may revert to a current-source behavior due to current saturation, making its instability mechanism more complex[16]. Therefore, targeted transient stability research on Grid-Forming Voltage Source Converters is necessary. Reference [17] investigates the impact of different parameters in grid-forming converters on transient stability and proposes a control strategy that adjusts the power reference to enhance stability. Study [18] improved transient stability via adaptive active power output switching in the converter control scheme, enabling dynamic response optimization during faults. Reference [19] enhances the transient synchronization stability in grid-forming converters systems through voltage magnitude adjustment. Reference [20] also presented an adaptive control algorithm in which both the Pref and Vref are adjusted in real time. This approach enhances power-angle stability and reduces steady-state current components during faults. However, the analysis did not account for current saturation effects. Given the inherent overcurrent limitations of power electronic devices, current saturation control must be incorporated into the control structure of grid-forming voltage source converters. Consequently, comprehensive transient stability analysis of GFM-VSCs under fault scenarios must explicitly incorporate current saturation dynamics. To investigate the effect of current limiting on grid-forming converters, Reference [21] conducted a systematic evaluation of its impact on transient synchronization stability under large-grid-disturbance conditions. Furthermore, an enhanced current saturation strategy was proposed to improve the system's transient stability performance. Reference [22] proposed an optimized grid-forming control strategy based on virtual impedance, which analytically derives the virtual impedance equations for steady-state fault current limitation in grid-forming converters under varying grid voltage sag depths. Building on this work, the authors developed an adaptive fault current limiting method using virtual impedance adaptation. In summary, regarding the rotor angle stability of grid-forming inverters under large disturbances, existing studies have yet to resolve the critical challenge of rapidly identifying post-fault stability. To prevent further deterioration of GFM-VSC system stability after faults and to strengthen the security and stability protection framework of renewable energy grids, this study begins by examining the dynamic behavior of conventional d-axis priority current limiting strategies under fault conditions using power-angle characteristics, thereby elucidating the transient synchronization stability in grid-forming voltage source converters under current saturation. considering the idea of relative kinetic energy in two-machine system, this paper suggests an instant emergency management technique to enhance the temporary stability of GFM-VSCs under current restriction circumstances. The real-time transient stability of the system is judged according to the trend of rotational speed deviation difference and power angle difference. Finally, the equal-area criterion calculates the active power adjustment that is needed. The simulation analysis of GFM-VSC.grid-connected system is carried out, and the simulation results verify the correctness of the theoretical analysis and the effectiveness of the proposed control method.

II. TRANSIENT SYNCHRONIZATION STABILITY ANALYSIS OF GRID-FORMING SYSTEMS UNDER LIMITATION CONSTRAINTS

A. GRID-CONNECTED INVERTER MODEL

The foundation of grid-forming control is establishing voltage source behavior in power converters, allowing it to actively provide voltage and frequency support to the grid. By simulating the power-angle characteristics of synchronous generators, the converter not only gains the ability to actively adjust phase, but also significantly improves power-angle stability and system synchronization. Among them, droop control and virtual synchronous generator (VSG) control simulate the speed regulation characteristics and swing equation of synchronous generators, respectively, and are the most used grid-forming control strategies. Based on the VSG control method, a control model for the grid-forming converter is established by simulating the external dynamic characteristics of synchronous generators.

1) TOPOLOGY OF GRID-FORMING CONVERTER SYSTEM

Figure 1 illustrates the main circuit topology and control block diagram of the grid-forming converter system. Udc is the DC side voltage of the converter; Lf and Cf are output filter inductance and capacitance; Upcc and iabc are the voltage and injected current at PCC; Ugabc is the grid voltage; iLabc is three-phase output current of the converter; Rg and Lg are resistance and inductance of the grid connection line. Reference phase θref and reference voltage magnitude Vref are introduced in the control system to simulate the performance of synchronous generator, and then the grid-forming control strategy is implemented.

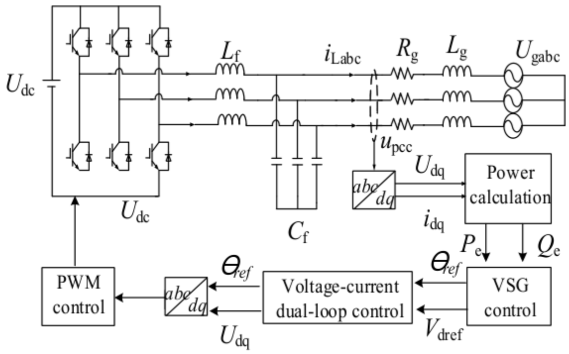

FIGURE 1. Main Circuit Topology and Control Block Diagram of the System

2) CONTROL STRATEGY OF GRID-FORMING CONVERTER

As shown in Figure 2 the Virtual Synchronous Generator VSG control includes two parts, one is active power-frequency control loop, another is reactive power-voltage control loop. The active power-frequency control loop simulates the rotor dynamic equation of SG, and obtain the frequency regulation characteristic and inertia response characteristic. The active power-frequency control loop emulates the rotor dynamics of a synchronous generator (SG), providing frequency regulation and inertial response capabilities. Meanwhile, the reactive power-voltage control loop replicates the excitation system behavior, delivering voltage support and reactive power control.

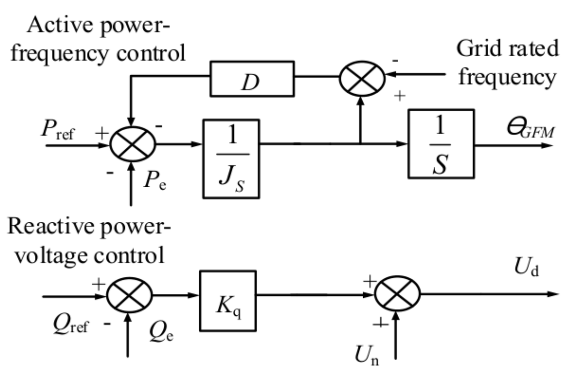

FIGURE 2. VSG Control Principle Block Diagram

The mathematical equations for establishing the power outer loop control are as follows:

$$J\frac{d\omega}{dt} = P_m - P_e - D(\omega - \omega_0) \quad (1)$$

$$U_d = U_n + K_q(Q_{\text{ref}} - Q_e) \quad (2)$$

D represents the damping coefficient; J is the moment of inertia; Pref and Qref respectively represent the reference value of active power and the reference value of reactive power; Pe and Qe respectively represent the active power and reactive power delivered by the converter to the grid; Kp and Kq respectively represent the active-frequency droop coefficient and reactive-voltage droop coefficient; ω_0 and ω respectively represent the reference angular frequency and the output angular frequency.

3) THE VIRTUAL POWER ANGLE OF THE INVERTER

Let δ denote the angle between the d-axis and the voltage vector U, representing the virtual power angle of the inverter. Then,

$$\frac{d\delta}{dt} = \omega - \omega_0 \quad (3)$$

The power angle of a conventional synchronous generator is defined as the angle between its internal voltage E and the grid voltage U, which represents the output power of the synchronous generator from the synchronous generator. As defined above, the virtual power angle of inverter reflects the output power of inverter under the steady-state condition. The reason for defining the virtual power angle as the angle between the d-axis and U is that the control equation of grid-connected converter directly determines the movement of d-axis, while the swinging equation of synchronous generator directly determines the movement of rotor angle, i.e. the phase of internal voltage E. It should be noted that, in steady state, the output voltage E of inverter is defined on the d-axis. Therefore, the virtual power angle and inverter power angle are equal. While, due to the influence of voltage outer loop dynamics, they are not equal in the transient process. Specifically, when the current is saturated, voltage outer loop has no impact on E, E no longer is on the d-axis. At this time, it is impossible to study the power angle, but the movement of virtual power angle δ can be directly derived from the droop equation, so the definition of virtual power angle is more meaningful in describing the synchronous state of inverter.

4) THE CHARACTERISTIC EQUATION OF THE INVERTER'S VIRTUAL POWER ANGLE

This paper primarily analyzes the motion changes of the virtual power angle δ under large disturbances. To this end, the electromagnetic transient process of the inverter and the control transient response process are simplified, with the following assumptions:

Assumption 1: Without loss of generality, it is assumed that under steady-state conditions, the composite vector of the inverter output voltage E is positioned on the d-axis and operates at a unity power factor.

Assumption 2: The effects of harmonic components, negative-sequence, and zero-sequence components are neglected.

Assumption 3: The resistance of the line and filter inductors is neglected, and the electromagnetic transient process of the filter inductors and lines is ignored. The impact of the capacitor current in the LC filter is also neglected.
Assumption 4: The inner current loop is sufficiently high in bandwidth to make its transient dynamics negligible.
Assumption 5: The voltage drop caused by the Q-V droop effect is neglected, and it is assumed that V = V0.
Assumption 6: Without loss of generality, the large disturbance analyzed in this paper comes from an external voltage magnitude drop. For other types of large disturbances leading to a shift in the operating point, the analysis process and conclusions are equally applicable. The output power expression of the inverter is:

$$P_E = \frac{EU}{X}\sin\delta \tag{4}$$

B. TRANSIENT SYNCHRONOUS STABILITY ANALYSIS CONSIDERING CURRENT LIMITING

For convenience in subsequent analysis, the state of the GFM-VSC is defined as follows:
(1) When the current amplitude of the GFM-VSC is less than the maximum limit Imax and it behaves as a controlled voltage source externally, it is defined to be in the normal operating state
(2) When the current amplitude of the GFM-VSC reaches Imax, the system enters the current-limiting control phase. At this point, the GFM-VSC behaves as a controlled current source externally, and it is defined to be in the current-limiting operating state.

1) CURRENT LIMITING CONTROL STRATEGY

Since overcurrent can lead to inverter damage, a current limiting mechanism is usually introduced in the control strategy to restrict the output current of the inverter. To achieve this, a current limiting block must be set in the GFM-VSC controller. Common limiting methods include dq-axis current proportional limiting and dq-axis current dynamic limiting. For the sake of analysis, this paper assumes, without loss of generality, that the inverter adopts the d-axis current priority limiting strategy (if other limiting methods are used, the analysis process and approach are similar). The specific control rate is as follows.

$$\begin{aligned} |I_{d,\mathrm{ref}}| &= \min\left(I_{\max}, \left|I^*_{d,\mathrm{ref}}\right|\right), \\ |I_{q,\mathrm{ref}}| &= \min\left(\sqrt{I^2_{\max} - I^2_{d,\mathrm{ref}}}, \left|I^*_{q,\mathrm{ref}}\right|\right) \end{aligned} \tag{5}$$

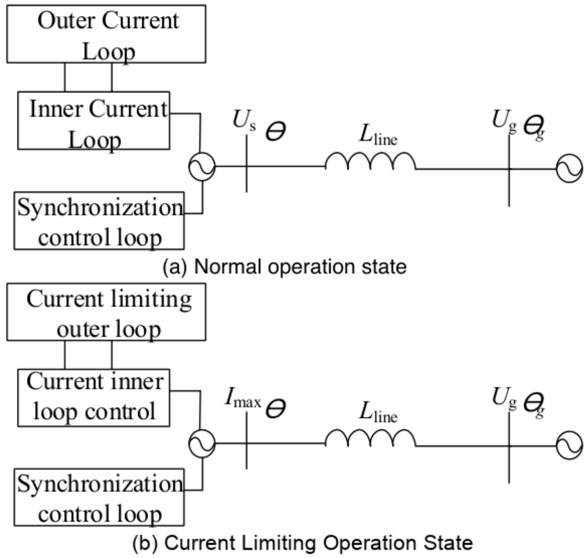

FIGURE 3. GFM-VSC Equivalent Circuit

In the equation, $I^*_{d,\mathrm{ref}}$ and $I^*_{q,\mathrm{ref}}$ are the d- and q-axis current reference values output by the voltage outer loop, respectively; $I_{d,\mathrm{ref}}$ and $I_{q,\mathrm{ref}}$ are the d- and q-axis current reference values output by the current limiting block. The conventional d-axis priority current limiting strategy restricts the current reference values, effectively controlling the output current magnitude of grid-forming inverters. In this strategy, the d-axis current component is prioritized during current limiting and is the first to reach the maximum allowable current value Imax, thereby enhancing the converter's active power transfer capability under fault conditions. Once the output current of the GFM-VSC is constrained to Imax, the current limiting control module is activated. As a result, the external equivalent behavior of the GFM-VSC transitions from voltage source mode to a controlled current source type. This dynamic process can be represented by the equivalent circuit diagram shown in Figure 3.

2) THE VIRTUAL POWER ANGLE CHARACTERISTICS UNDER INVERTER CURRENT SATURATION

The power angle of a traditional synchronous generator is defined as the angle between its internal electromotive force and the grid voltage. It reflects the magnitude of the generator's output power. For a grid-forming energy storage system, its power angle, known as the virtual power angle, is defined in this paper as the angle between its d-axis and the grid voltage vector, as shown in Figure 4. This angle can be regarded as the power angle of the grid-forming energy storage device. When the system is in steady state, the output voltage of the grid-forming energy storage device is positioned along the d-axis, similar to the power angle definition of traditional synchronous machines, and it can also reflect the output power of the grid-forming energy storage device. When the system enters a transient process, due to the dynamics of the voltage outer loop, the virtual power angle does not coincide with the power angle of traditional synchronous machines. If, after a fault, the system voltage drops to a level where the output current of the grid-forming energy storage device reaches the current limit, the voltage outer loop becomes ineffective, and the output voltage of the grid-forming energy storage device shifts off the d-axis. In this case, the power angle of the grid-forming energy storage device cannot be directly studied. However, since the grid-forming strategy used in this paper is based on a d-axis priority current limiting strategy, which ensures that the d-axis current Id increases first and reaches the maximum current limit Imax, the description of the virtual power angle during the transient period still holds theoretical significance.

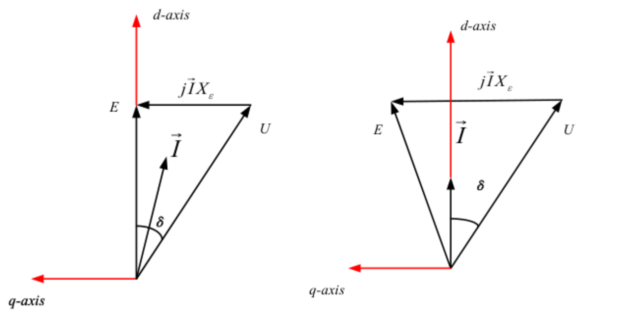

FIGURE 4. dq-Axis Vector Diagram of Grid-Forming Energy Storage Device

When the output current saturates, under the d-axis current priority limiting control strategy, the d-axis current gradually increases to the maximum allowable value Imax, while the q-axis current gradually decreases to zero. Therefore, the output power expression of the inverter under current saturation can be formulated as follows:

$$P_e = U_g I_{\max} \cos\delta \tag{6}$$

According to the equation, we can obtain the power angle characteristic curves of the normal operating state and the current-limiting operating state respectively. Because of Imax, the limitation of the peak value of the current-limiting curve is smaller than that of the normal operating curve. When the GFM-VSC operates in the current-limiting state, the system may not have a stable operating point; therefore, faults should be cleared quickly to ensure system stability. When the grid voltage drops to a deep level, the system may lose its stable operating point, as indicated by the red dashed line in Figure 5. At this time, the system cannot operate stably.

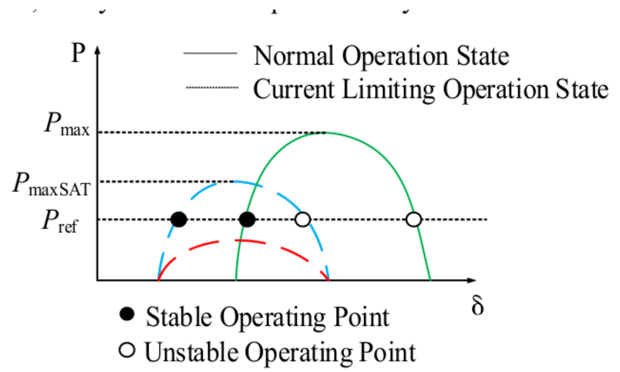

FIGURE 5. The Power Angle Characteristic Curve under Normal Operating Conditions and under Limited Amplitude Operating Conditions

3) TRANSIENT STABILITY MECHANISM ANALYSIS OF THE INVERTER'S VIRTUAL POWER ANGLE

From the above analysis, the grid-forming energy storage device, under normal operating conditions, exhibits power response characteristics identical to those of traditional synchronous generators. After the current-limiting block is triggered, as indicated in Equation (6), the output power of the grid-forming energy storage device is related to the grid voltage drop magnitude. The angular component of its output active power changes from a sine wave to a cosine wave, reflecting the transition of the control mechanism from a voltage source characteristic to a current source characteristic. This paper further compares and analyzes the transient response process of the grid-forming energy storage system under normal operating conditions and current-limiting conditions. The relevant processes are shown in Figures 6, where Pmax represents the maximum output active power of the grid-forming energy storage device under current-limiting conditions. In steady-state, the power angle curve of the grid-forming energy storage device is shown by the blue curve in Figure 6, with the system equilibrium point at a. After a fault occurs, the voltage magnitude U of the external grid drops. Since the inverter cannot provide short-circuit current like a traditional synchronous generator, and instead becomes a current source under current-limiting, the operating point of the inverter will switch from the non-limiting virtual curve to the current-limited virtual curve. Additionally, from Figure 6, it can be observed that due to current-limiting, the region of the virtual power angle curve beyond point e is unreachable, as this would require the inverter's output current to exceed Imax, which contradicts the current-limiting constraint. Following a system disturbance, the operating condition evolves from its initial state a to b, and the operating point will then move along the red curve towards increasing δ_{GFM}. If the issue is resolved at stage c, the power angle characteristic curve of the constructive energy storage device will change from red to blue, and the system operating point will also move from point c to point d. Since the kinetic energy of the virtual synchronous generator still maintains a positive value, the virtual power angle will continue to rise until it reaches point e. At this stage, the inverter will enter current limiting mode, and the power angle characteristic curve will then switch from blue to green, continuing to evolve along the green curve. If before reaching point h, the virtual synchronous machine's kinetic energy has not yet decreased to zero, the virtual power angle will continue to increase along the green curve, and the grid-forming energy storage device will experience transient instability, with the virtual power angle failing to return to a stable operating point. If, before point h, the virtual synchronous machine's kinetic energy decreases to zero, δ_{GFM} will swing back, and after the dynamic process, the system operating point will return to the blue curve, eventually returning to the stable point at a. The system operating state will follow the cyclic path a →b →c →d →e →f before returning along the trajectory f →e →d →a. If the issue is resolved at stage g, and the power angle surpasses its maximum value, the color of the grid-forming energy storage device's characteristic curve shifts from red to green, effectively moving the system's operational point from g to f. Given that the virtual synchronous machine still possesses kinetic energy, the virtual power angle will keep climbing until it hits point h. Should the kinetic energy of the virtual synchronous machine not dip below zero prior to reaching h, the virtual power angle will shoot past h, leading to transient instability in the grid-forming energy storage device. This instability would prevent the device from reestablishing its stable operating point. If, before h, the virtual power angle's kinetic energy decreases to zero, δ_{GFM} will swing back to point e, at which point I<Imax, the grid-forming device exits the current-limiting state, and the power angle characteristic curve switches from green to blue, eventually reaching the stable point a. The system operating point will follow the path a →b →c →g →f →e →d →a. If the issue gets resolved at point i and the current exceeds the maximum limit, the power angle characteristic curve for the grid-connected energy storage system flips from red to green. Consequently, the operational point shifts from i to j. At j, the power output is less than the reference level, leading to a sustained rise in the virtual synchronous machine's kinetic energy. This prevents the virtual power angle from re-establishing the stable equilibrium. The grid-forming energy storage device will experience transient instability. To avoid this, the fault should be cleared promptly at h, or appropriate measures should be taken.

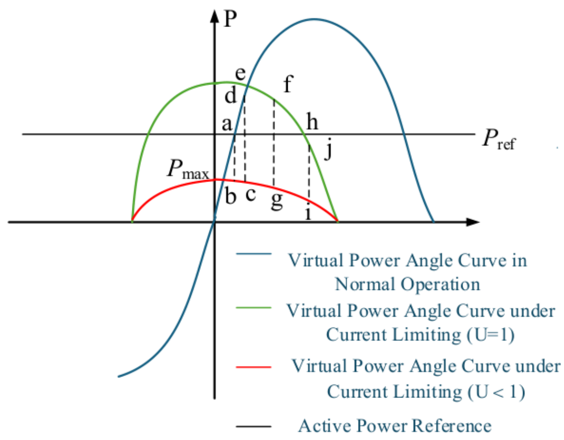

FIGURE 6. The Virtual Power Angle Curve of the Grid-Forming Energy Storage Device

III. TRANSIENT STABILITY REAL-TIME EMERGENCY CONTROL SCHEME BASED ON RELATIVE KINETIC ENERGY

A. REAL-TIME EMERGENCY CONTROL BASED ON RELATIVE KINETIC ENERGY

For a single-machine infinite bus system, the rotor motion equation of the grid-forming generator is:

$$\begin{aligned} \frac{d\delta}{dt} &= \Delta\omega\,\omega_0, \\ \frac{d\omega}{dt} &= \frac{1}{T_j}(P_m - P_e) \end{aligned} \tag{7}$$

PI, PII, and PIII correspond to the generator power characteristic curves before, during, and after the fault, respectively. The power angle reaches δ_c when the fault is cleared. When the generator power angle reaches δ_d, the remaining acceleration area (referring to the total acceleration area minus the deceleration area already covered) can be expressed as:

$$\begin{aligned} S_{\mathrm{remain}} &= \int_{\delta_0}^{\delta_c} (P_m - P_{\mathrm{II}})\,d\delta + \int_{\delta_c}^{\delta_d} (P_m - P_{\mathrm{III}})\,d\delta \\ &= \frac{1}{2}T_j\omega_0\Delta\omega^2\Big|_{\delta_0}^{\delta_c} + \frac{1}{2}T_j\omega_0\Delta\omega^2\Big|_{\delta_c}^{\delta_d} \\ &= \frac{1}{2}T_j\omega_0\Delta\omega_d^2 \end{aligned} \tag{8}$$

The term Sremain represents the remaining acceleration area corresponding to the system's operation at the current moment. When it is determined that the system will lose power angle stability, an emergency transient stability control scheme can be activated. The control strategy involves subtracting the remaining deceleration area from the remaining acceleration area to calculate the deceleration area deficit, which is used to determine the control machine-out quantity. From equation (8), it can be observed that relative kinetic energy does not have actual physical significance. There is no corresponding physical quantity, and it is merely the squared difference in rotational speeds, referred to as relative kinetic energy, which represents the remaining acceleration area.

B. CALCULATION OF POWER CHARACTERISTIC CURVE BASED ON RELATIVE KINETIC ENERGY

The power curve of a Virtual Synchronous Machine is given by:

$$P_e = \begin{cases} \dfrac{EU}{X}\sin\bar{\delta}, & \text{non-saturated current,} \\ UI_{\max}\cos\bar{\delta}, & \text{saturated current} \end{cases} \tag{9}$$

The relative kinetic energy at time t and t+1 is calculated, and the difference between them represents the deceleration area the system has undergone during this period. This deceleration area is approximated as a rectangle, which allows the calculation of ΔP for this time interval.

$$\Delta P = \frac{W_t - W_{t+1}}{\bar{\delta}_{t+1} - \bar{\delta}_t} \tag{10}$$

$$P_e = P_{\text{ref}} + \Delta P \tag{11}$$

In practical systems, if Pref of the grid-connected system can be obtained, it can be substituted into equation (11) to obtain discrete points of the power characteristic curve. Starting from the moment of fault clearance, the value of Pet is calculated at each moment to obtain a series of discrete points on the power characteristic curve. When it is identified that the system will lose stability, the least squares method can be used with all the existing discrete points to synthesize the form of equation (9), which allows the estimation of the remaining deceleration area and provides a basis for adjusting Pref of the grid. The traditional calculation method uses a data window over a period of time to predict the power characteristic curve, as it requires comparing the acceleration and deceleration areas to assess the system's stability. In this method, the power characteristic curve is fitted using all available data. In fact, due to the influence of various factors, this method is only an approximation to a certain extent. The purpose of the fitting is to estimate the remaining deceleration area. In emergency control, reducing the active power reference not only decreases the mechanical power input but also affects the system's impedance. Achieving an accurate power characteristic curve is quite challenging. Therefore, a cyclic monitoring control approach is adopted, continuously evaluating the system's operation. If a single adjustment does not stabilize the system, further adjustment control is applied.

C. CONTROL DECISION ALGORITHM

Clearly, through the discussion in Section 3.2, the power characteristic curve of the equivalent system has been obtained. By applying the equal-area criterion for the two-machine system, the control quantity for adjusting the active power reference value can be calculated. The overall schematic is shown in Figure 7.

verall schematic is shown in Figure 7.

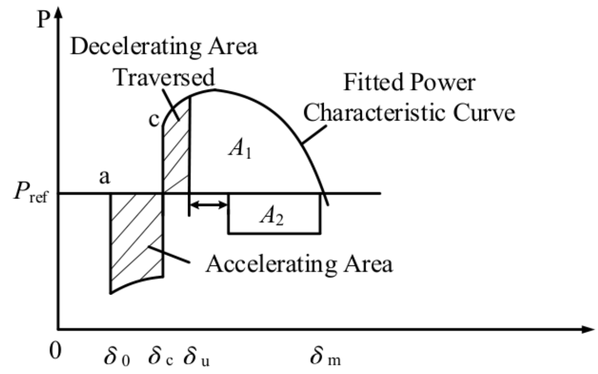

FIGURE 7. Schematic Diagram of Control Decision-Making

When instability is detected in the system, the remaining acceleration area at that moment is first calculated. In Figure 7, A1 represents the remaining deceleration area estimated based on the fitted power characteristic curve. Due to the insufficient deceleration area, the deceleration area that needs to be increased after control implementation is given by:

$$S_c = S_{\text{remain}} - S_d = \frac{1}{2}\omega_0 \Delta\omega_{\bar{\delta}_u}^2 - \int_{\bar{\delta}_u}^{\bar{\delta}_m} (P_e - P_m)\, d\bar{\delta} \tag{12}$$

The actual control process involves time delays that must be considered for their impact on control effectiveness. These time delays consist of three parts: control decision time, data and control command transmission time, and the actual controller action time. Since system stability identification and power characteristic curve fitting are performed simultaneously, control measures can be determined quickly once the system instability is identified. The primary time delay is due to control action implementation and data transmission. Assuming the control action time is 50 ms, control decision time is 10 ms, and data transmission time is 40 ms, the total delay time is 100 ms. Therefore, the actual control action time does not correspond to the exact moment the system instability is identified. To account for this effect and obtain a more reasonable machine-out quantity, the control quantity calculation formula is:

$$\Delta P_m = \frac{S_c}{\bar{\delta}_m - \bar{\delta}_u - \Delta\omega_u t_{\text{delay}}} \tag{13}$$

After calculating the total reduced Pref, Pref are adjusted according to the output conditions in the accelerating machine group.

D. THE OVERALL FRAMEWORK FLOW

This paper assumes that the entire system has measurement and communication capabilities. The flow of the real-time emergency control scheme for transient power angle stability based on relative kinetic energy is shown in Figure (8).

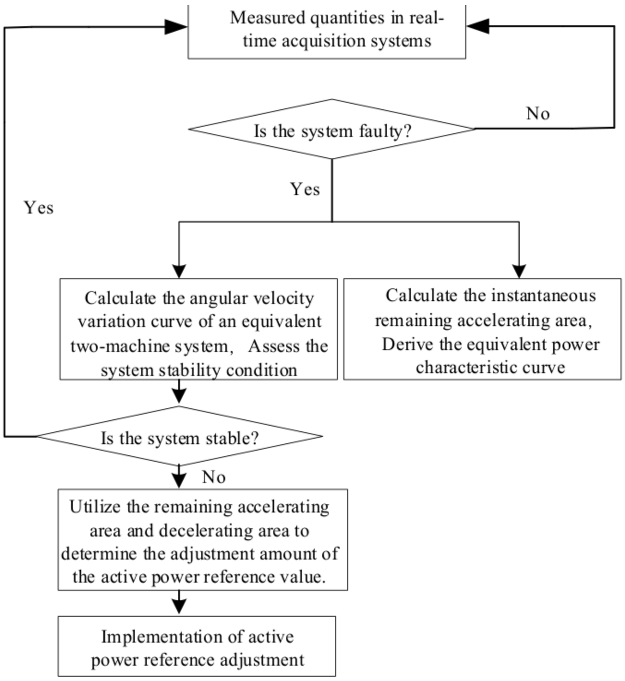

FIGURE 8. Real-Time Emergency Control Overall Process

When it is determined that the system will eventually become unstable, it is necessary to prevent system instability by adjusting the Pref of the grid-connected system. After implementing the adjustment, the output of the prime mover is reduced, allowing more rotor kinetic energy to be transferred between the two potentials as the power angle swings. This enhances the mutual attraction between the two potentials, suppressing the increasing trend of the speed difference and power angle difference, which is beneficial for maintaining synchronous stability. Since a single adjustment control may not guarantee system stability, a feedback-based closed-loop control is employed. The system response is continuously monitored to determine if emergency control needs to be reinitiated.

IV. RESULTS

To validate the proposed control strategy and the transient analysis of the grid-connected energy storage converter under disturbances, a simulation model was built using the MATLAB/Simulink platform, as shown in Figure (1).

A. CASE 1: SUDDEN GRID VOLTAGE SAG

The grid-connected energy storage device is set with an output current limit Imax=0.26 p.u., and the active power reference value is Pref=0.23 p.u. A fault occurs at t=0.3 s, during which the system voltage magnitude is Ug=0.6 p.u., and the fault is cleared at t=0.39 s.

The simulation results are shown in Figure 9. Curve a and curve b represent the rotor speed curve and rotor angle swing curve of the virtual synchronous machine, respectively. Curve c represents the active power reference value curve of the virtual synchronous machine, curve d is the phase plane trajectory, and curves e and f represent the virtual synchronous machine's power angle curves under conditions without and with emergency control, respectively. As seen from the figure, at t = 0.41 s, the system is identified as being on the verge of losing stability. At this point, the remaining acceleration area, calculated using the relative kinetic energy formula, is 0.1046, while the remaining deceleration area obtained through the fitting method is 0.0732. The required adjustment in active power increment, calculated using equation (13), is $\Delta Pm = 0.006$. Therefore, the active power reference value of the grid-connected energy storage device is reduced by 0.006 p.u., and the actual control action is implemented at t = 0.51 s. From the simulation results, it can be observed that after the power adjustment measures are taken, the increase in the virtual power angle is effectively suppressed, and it begins to stabilize, keeping the system in a synchronized operating state. In contrast, without the emergency control strategy, the system's speed and rotor angle both show a significant divergent trend, indicating inadequate transient stability of the system. after the emergency control is applied at t = 0.51 s, the speed deviation and rotor angle swing are significantly reduced, and the system gradually stabilizes. The rapid adjustment of active power effectively suppressed power fluctuations and enhanced the system's power balance ability. Furthermore, the phase plane trajectory (Figure d) clearly shows that the system's state trajectory converges towards a stable equilibrium point after the emergency control is introduced, further verifying the effectiveness of the proposed emergency control strategy. in summary, the simulation results demonstrate that the proposed emergency control strategy can significantly improve the transient stability performance of the virtual synchronous machine system.

B. CASE 2: WHEN THE FIRST EMERGENCY CONTROL SCHEME FAILS TO RESOLVE THE ISSUE

When the fault type and operating scenario are the same as in case 1, but the initial emergency control scheme fails to effectively suppress the system's transient instability, the real-time monitoring system will once again identify the risk of the system losing stability. In this case, the system triggers the secondary emergency control mechanism and implements the corrected control measures. After the failure of the initial emergency control measures, the secondary emergency control is activated. Due to the influence of control and execution delays, the system is identified at t = 0.51 s as being on the verge of transient instability once again. At this moment, the remaining acceleration area, calculated using the relative kinetic energy criterion, is 0.0745, while the remaining deceleration area obtained from the fitted equivalent power characteristic curve is 0.0561. The required active power adjustment, calculated using equation (13), is $\Delta Pm = 0.009$. Therefore, the active power reference value of the grid-connected energy storage system is reduced by 0.009 p.u., and the corresponding physical control action is executed at t = 0.61 s. After the control

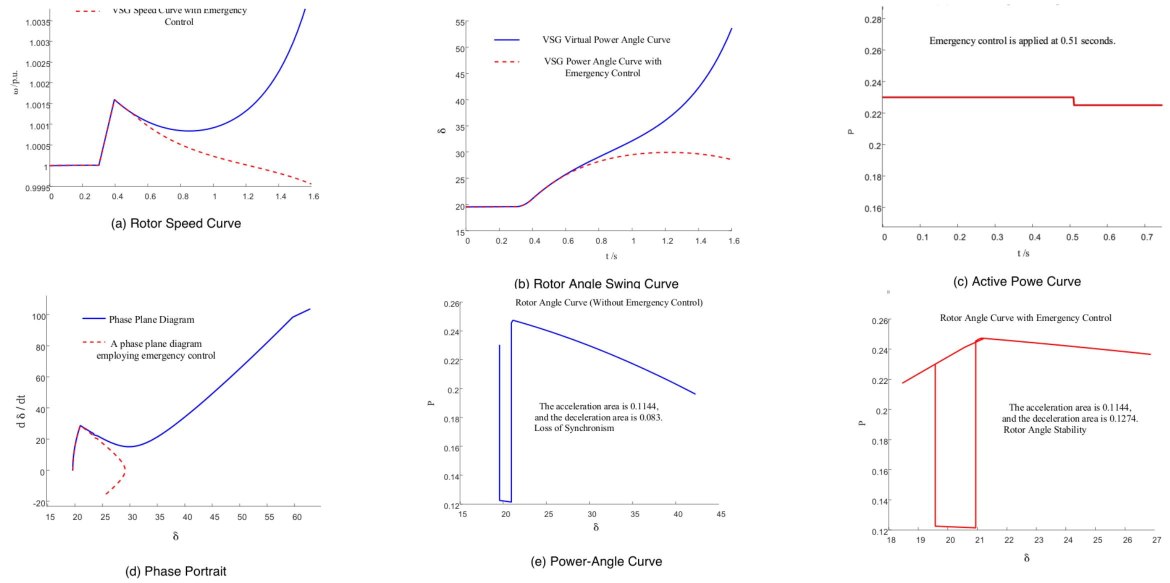

FIGURE 9. Power Angle Stability Simulation Curves of Grid-Forming Devices

measures are applied, the system's dynamic response is significantly improved. As shown in Figure 10(b), the virtual power angle, after a brief rise, reverses its growth trend and gradually decreases, with the system ultimately returning to a stable operating state. Meanwhile, Figure 10(a) shows that the speed deviation is effectively suppressed, preventing the system from continuously accelerating and causing instability. From the phase plane trajectory (Figure 10(d)), it can be further observed that, without emergency control, the system's state trajectory shows a clear divergence. However, after the secondary emergency control strategy is applied, the system's trajectory gradually converges towards a stable equilibrium point, indicating that the system's phase space stability is significantly enhanced.

In summary, the simulation results demonstrate that the emergency control strategy based on the equivalent power characteristic curve and remaining kinetic energy criterion is still effective in compensating for the failure of the initial control through secondary intervention. The rapid adjustment of active power output significantly improves the transient stability performance of the virtual synchronous machine system.

C. CASE 3: WHEN THE VOLTAGE FAULT FURTHER DROPS

Under the same operating scenario, the voltage fault magnitude is further increased to a drop of 0.5 p.u. to assess the ability of the proposed control strategy to support the system's transient stability under more severe operating conditions. The corresponding simulation results are shown in Figure 11. From Figure 11, it can be seen that as the fault duration is extended, the system's transient response becomes significantly more severe. At t =0.41 s, both the virtual speed and virtual power angle of the virtual synchronous machine exhibit a clear divergent trend, indicating that the system is gradually approaching the critical state of losing transient stability. Based on the relative kinetic energy instability criterion, the remaining acceleration area at this point is calculated to be 0.1838, while the remaining deceleration area obtained from the fitted equivalent power characteristic curve is 0.0688. The required active power adjustment, calculated using equation (13), is $\Delta Pm = 0.02$. Therefore, the active power reference value of the grid-connected energy storage system is reduced by 0.02 p.u., and this control action takes effect at t = 0.51 s. From the simulation results, it can be clearly observed that after the power adjustment measures are implemented, the increasing trend of the virtual power angle is effectively suppressed, and it gradually reverses, showing a decreasing trend. At the same time, the system's speed response becomes noticeably smoother. Therefore, even under a more severe fault, the system is still able to successfully avoid power angle divergence and frequency instability, maintaining a stable operating state. In summary, the simulation results show that the emergency control strategy, based on the equivalent power characteristic curve and remaining kinetic energy criterion, can intervene in a timely manner before the system becomes unstable. By rapidly adjusting the active power output, it effectively improves the transient stability performance of the virtual synchronous machine system under severe fault conditions.

D. CASE 4: WHEN THE CURRENT LIMITING CAPABILITY IS WEAKENED

Under the same fault type and operating scenario, the overcurrent capability of the grid-forming converter is adjusted by setting the current limit to Imax = 0.25 p.u. to assess the transient stability support ability of the proposed control

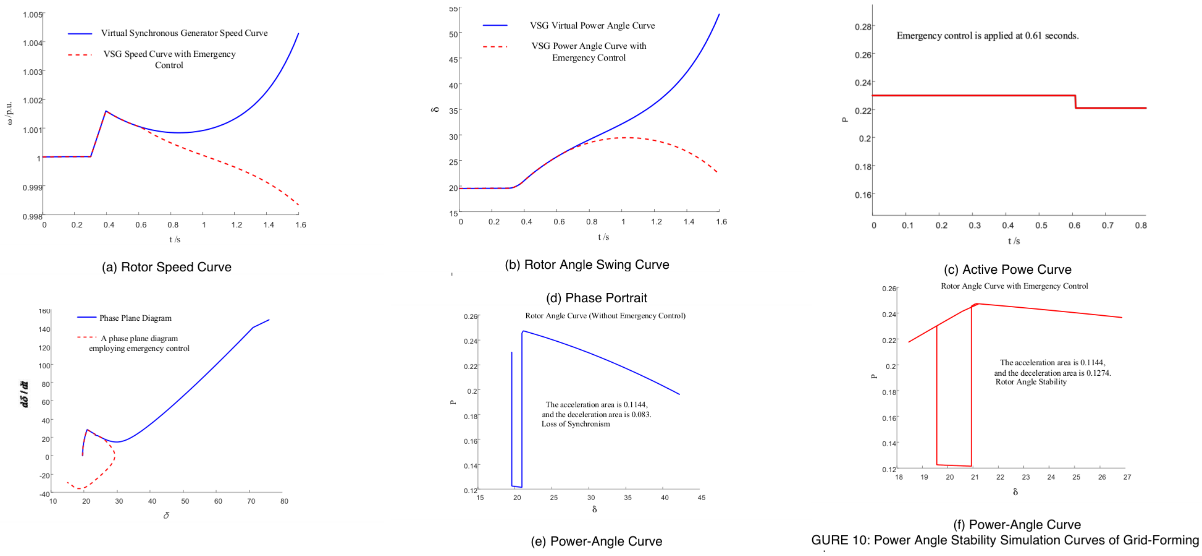

FIGURE 10. Power Angle Stability Simulation Curves of Grid-Forming Devices

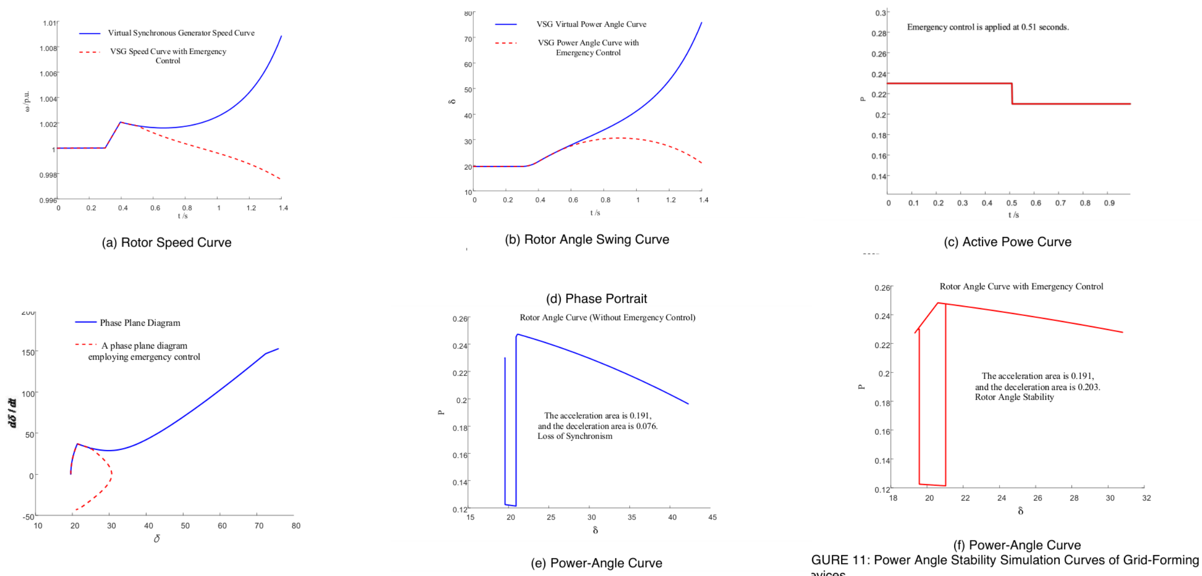

FIGURE 11. Power Angle Stability Simulation Curves of Grid-Forming Devices

strategy. The corresponding simulation results are shown in Figure 12. From Figure 12, it can be observed that as the fault duration is extended, the system's transient response becomes significantly more severe. At approximately t = 0.41 s, both the virtual speed and virtual power angle of the virtual synchronous machine exhibit a noticeable divergent trend, indicating that the system is approaching transient instability. Based on the relative kinetic energy instability criterion, the remaining acceleration area at this point is calculated to be 0.124, while the remaining deceleration area obtained from the fitted equivalent power characteristic curve is 0.002. According to equation (13), the required active power adjustment is $\Delta Pm = 0.021$. Therefore, the active power reference value of the grid-connected energy storage system is reduced by 0.044 p.u., and the corresponding control action takes effect at t = 0.51 s. It is clearly observed that after the power adjustment measures are implemented, the increasing trend of the virtual power angle is effectively suppressed, and it gradually reverses to a decreasing trend. Meanwhile, the speed response becomes much smoother. As a result, the system successfully avoids power angle divergence and frequency instability, maintaining stable operation even with an extended fault duration. The simulation results indicate that the proposed emergency control strategy can significantly improve the transient stability performance of the VSG system.

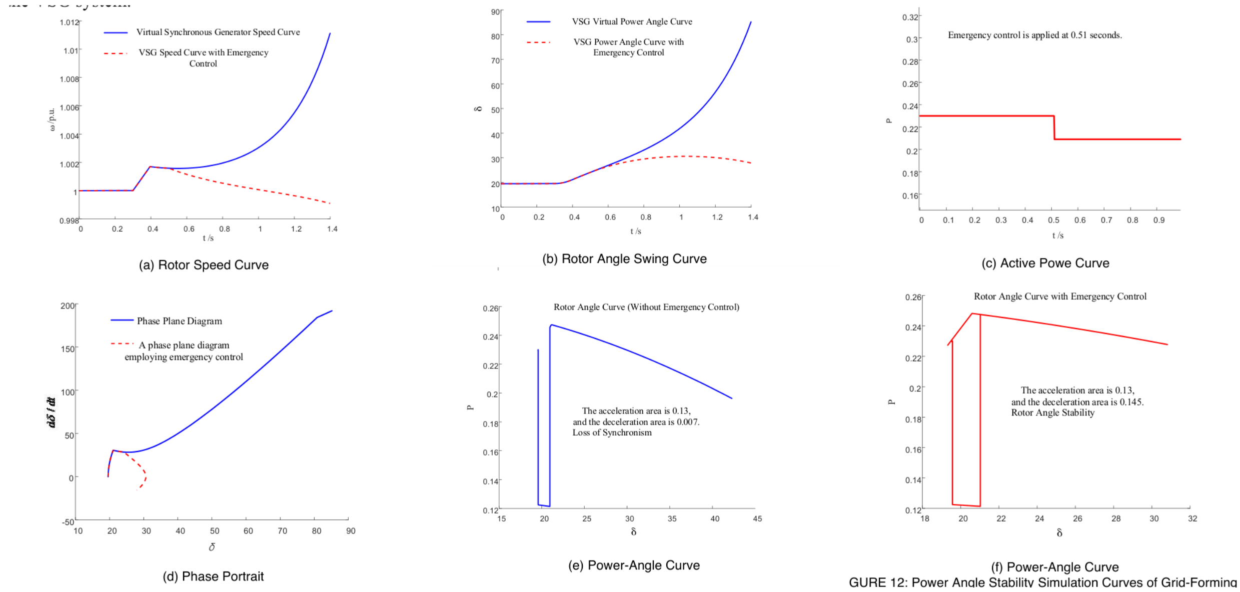

FIGURE 12. Power Angle Stability Simulation Curves of Grid-Forming Devices

V. CONCLUSION

Under grid voltage sag fault conditions, the proposed adaptive control strategy based on relative kinetic energy successfully identifies the risk of transient instability in the system. By calculating the difference between the accelerating and decelerating areas in real time, it accurately generates an active power adjustment command. Simulation results show that the increasing trend of the virtual power angle is reversed after the adjustment, and system stability is restored, verifying the effectiveness of the strategy under a single fault.

When the initial control action fails to fully eliminate the instability, the system triggers a secondary control through a closed-loop monitoring mechanism. Despite the presence of time delays, stability is recovered through recalculated adjustments, demonstrating the strategy's robustness and fault tolerance in dealing with control failures or complex fault scenarios, thereby preventing further deterioration of the situation. This highlights its significant practical value in engineering applications. Essentially, the method operates as a feedback control mechanism. Although its intervention may be delayed, it offers flexibility, effectiveness, and strong adaptability, serving as a complementary measure to traditional security and stability control systems. Case studies confirm that the proposed method features low computational burden, high flexibility, and strong reliability, thereby establishing a new defense line to prevent large-scale blackouts and demonstrating considerable practical value in engineering applications.

ACKNOWLEDGEMENT

We acknowledge the linguistic support received during the preparation of this manuscript.

FUNDING STATEMENT

This work was supported by the Project of Research and Application of Post-Fault Stability Response Analysis and Intelligent Simulation Diagnosis Technology for New-Type Power Systems under Grant No. 000005KC24010001.

AVAILABILITY OF DATA AND MATERIALS

The authors confirm that the data supporting the findings of this study are available within the article.

ETHICS APPROVAL

Not applicable.

CONFLICTS OF INTEREST

The authors declare no conflicts of interest to report regarding the present study.

NOMENCLATURE

VSC	Voltage Source Converter
GFL	Grid-following
GFM	Grid-forming
VSG	Virtual Synchronous Generator

REFERENCES

[1] C. Zou, Q. Zhao, G. Zhang, and B. Xiong, "Energy revolution: From a fossil energy era to a new energy era," Nat. Gas Ind. B, vol. 3, no. 1, pp. 1–11, 2016, DOI: 10.1016/j.ngib.2016.02.001.
[2] Y. Zhang, P. Denholm, D. Arent, and S. F. Baldwin, "The challenges of achieving a 100% renewable electricity system in the United States," Joule, vol. 5, no. 6, pp. 1331–1352, 2021, DOI: 10.1016/j.joule.2021.03.028.
[3] L. Xiong, X. Liu, Y. Liu, and F. Zhuo, "Modeling and stability issues of voltage-source converter-dominated power systems: a review," CSEE J. Power Energy Syst., vol. 8, no. 6, pp. 1530–1549, 2022, DOI: 10.17775/CSEEJPES.2020.03590.
[4] M. Barnes and A. Beddard, "Voltage source converter HVDC links—the state of the art and issues going forward," Energy Procedia, vol. 24, pp. 108–122, 2012, DOI: 10.1016/j.egypro.2012.06.092.

[5] X. Fu, J. Sun, M. Huang, Z. Tian, H. Yan, H. H.-C. Iu, P. Hu, and X. Zha, "Large-signal stability of grid-forming and grid-following controls in voltage source converter: a comparative study," IEEE Trans. Power Electron., vol. 36, no. 7, pp. 7832–7840, 2021, DOI: 10.1109/TPEL.2020.3047480.
[6] X. Gao, D. Zhou, A. Anvari-Moghaddam, and F. Blaabjerg, "A comparative study of grid-following and grid-forming control schemes in power electronic-based power systems," Power Electron. Drives, vol. 8, no. 1, pp. 1–20, 2023, DOI: 10.2478/pead-2023-0001.
[7] B. Hu, C. Zhao, S. Sahoo, C. Wu, L. Chen, H. Nian, and F. Blaabjerg, "Synchronization stability enhancement of grid-following converter under inductive power grid," IEEE Trans. Energy Convers., vol. 38, no. 2, pp. 1485–1488, 2023, DOI: 10.1109/TEC.2023.3265518.
[8] H. Zhang, W. Xiang, W. Lin, and J. Wen, "Grid forming converters in renewable energy sources dominated power grid: control strategy, stability, application, and challenges," J. Mod. Power Syst. Clean Energy, vol. 9, no. 6, pp. 1239–1256, 2021, DOI: 10.35833/MPCE.2021.000257.
[9] M. Khan, W. Wu, and L. Li, "Grid-forming control for inverter-based resources in power systems: a review on its operation, system stability, and prospective," IET Renew. Power Gener., vol. 18, no. 6, pp. 887–907, 2024, DOI: 10.1049/rpg2.12991.
[10] D. B. Rathnayake, M. Akrami, C. Phurailatpam, S. P. Me, S. Hadavi, G. Jayasinghe, S. Zabihi, and B. Bahrani, "Grid forming inverter modeling, control, and applications," IEEE Access, vol. 9, pp. 114781–114807, 2021, DOI: 10.1109/ACCESS.2021.3104617.
[11] S. Fazal, E. Haque, M. T. Arif, and A. Gargoom, "Droop control techniques for grid forming inverter," in Proc. Asia-Pacific Power Energy Eng. Conf. (APPEEC), 2022, pp. 1–6, DOI: 10.1109/APPEEC53445.2022.10072251.
[12] S. A. Khan, M. Wang, W. Su, G. Liu, and S. Chaturvedi, "Grid-forming converters for stability issues in future power grids," Energies, vol. 15, no. 14, 2022, Art. no. 4937, DOI: 10.3390/en15144937.
[13] R. Majumder, A. Ghosh, G. Ledwich, and F. Zare, "Angle droop versus frequency droop in a voltage source converter based autonomous microgrid," in Proc. IEEE Power & Energy Society General Meeting, 2009, pp. 1–8, DOI: 10.1109/PES.2009.5275987.
[14] K. M. Cheema, K. K. Mehmood, S. U. Khan, et al., "A comprehensive review of virtual synchronous generator," Int. J. Electr. Power Energy Syst., vol. 120, 2020, Art. no. 106006, DOI: 10.1016/j.ijepes.2020.106006.
[15] J. Wang, B. Ma, Q. Chen, Y. Cui, X. Chen, Y. Zhao, J. L. Ping, Y. Zhao, et al., "A comprehensive review of grid-forming control studies based on virtual synchronous generators," in Proc. 2024 7th Int. Conf. Energy, Electr. Power Eng. (CEEPE 2024), 2024, Art. no. 10586502, DOI: 10.1109/CEEPE62022.2024.10586502.
[16] Y. Zhang and A. E. Motter, "Symmetry-Independent Stability Analysis of Synchronization Patterns," SIAM Rev., vol. 62, no. 4, pp. 917–941, 2020, DOI: 10.1137/19M127358X.
[17] H. Wu and X. Wang, "A Mode-Adaptive Power-Angle Control Method for Transient Stability Enhancement of Virtual Synchronous Generators," IEEE J. Emerg. Sel. Topics Power Electron., vol. 8, no. 2, pp. 1034–1049, 2020, DOI: 10.1109/JESTPE.2020.2976791.
[18] Z. Shuai, C. Shen, X. Liu, Z. Li, and Z. J. Shen, "Transient Angle Stability of Virtual Synchronous Generators Using Lyapunov's Direct Method," IEEE Trans. Smart Grid, vol. 10, no. 4, pp. 4648–4661, 2019, DOI: 10.1109/TSG.2018.2866122.
[19] W. Si and J. Fang, "Transient Stability Improvement of Grid-Forming Converters Through Voltage Amplitude Regulation and Reactive Power Injection," IEEE Trans. Power Electron., vol. 38, no. 10, pp. 12116–12125, 2023, DOI: 10.1109/TPEL.2023.3290170.
[20] D. Pan, X. Wang, F. Liu, and R. Shi, "Transient Stability of Voltage-Source Converters With Grid-Forming Control: A Design-Oriented Study," IEEE J. Emerg. Sel. Topics Power Electron., vol. 8, no. 2, pp. 1019–1033, 2020, DOI: 10.1109/JESTPE.2019.2946310.
[21] T. Liu, X. Wang, F. Liu, K. Xin, and Y. Liu, "Transient Stability Analysis for Grid-Forming Inverters Transitioning from Islanded to Grid-Connected Mode," IEEE Open J. Power Electron., vol. 3, pp. 419–432, 2022, DOI: 10.1109/OJPEL.2022.3189801.
[22] X. Hu, Z. Li, C. Pan, H. Li, and Y. Liang, "An Adaptive Virtual-Impedance-Based Current-Limiting Method with the Functionality of Transient Stability Enhancement for Grid-Forming Converter," Electronics, vol. 13, 2024, Art. no. 2750, DOI: 10.3390/electronics13142750.